Hindawi Publishing Corporation
Journal of Nanomaterials
Volume 2014, Article ID 207258, 11 pages
http://dx.doi.org/10.1155/2014/207258

Research Article

Spectroscopic Identification of Neurotoxin Tetramethylenedisulfotetramine (TETS) Captured by Supramolecular Receptor β-Cyclodextrin Immobilized on Nanostructured Gold Surfaces

H. Dernaika,[1,2,3] S. V. Chong,[2,3] C. G. Artur,[1,2] and J. L. Tallon[2,3]

[1] *School of Chemical and Physical Sciences, Victoria University of Wellington, P.O. Box 600, Wellington 6140, New Zealand*
[2] *The MacDiarmid Institute for Advanced Materials and Nanotechnology, Victoria University of Wellington, P.O. Box 600, Wellington 6140, New Zealand*
[3] *Robinson Research Institute, Victoria University of Wellington, P.O. Box 33436, Lower Hutt 5046, New Zealand*

Correspondence should be addressed to H. Dernaika; haissamdern@gmail.com and
J. L. Tallon; jeff.tallon@callaghaninnovation.govt.nz

Received 6 November 2013; Revised 13 February 2014; Accepted 27 February 2014; Published 26 May 2014

Academic Editor: Miguel A. Correa-Duarte

We report on the spectroscopic identification of tetramethylenedisulfotetramine (TETS), a deadly neurotoxic rodenticide, captured on plasmonic substrates using supramolecular guest-host functionality. Commercial nanopatterned surface-enhanced Raman spectroscopy (SERS) active substrates were self-assembled with host β-cyclodextrin (CD) and the captured TETS was readily identified by X-ray photoelectron (XPS) and infrared spectroscopy, but not with Raman. Density functional theory (DFT) calculation was carried out to determine the Raman scattering cross section of TETS to gauge its Raman scattering efficiency in the preresonant 633 nm excitation region. This was found to be lower than 10^{-29} cm^2/sr, much lower than that of a dye molecule commonly used in SERS experiment. We explain the nondetection of TETS by Raman based on a combined intrinsically weak Raman scattering cross section and their low surface concentration, where XPS only shows a surface coverage of less than 0.02 monolayer with respect to the total number of gold sites. Comparing this to our own CD-decorated 10 nm gold nanoparticles (NPs) surface, we found that the inherently greater surface area provided by the NPs increases the amount of CD present (per unit area), giving our surface the capability to detect both the receptor and TETS via attenuated total reflectance (ATR) FTIR.

1. Introduction

Trace analytics delivering reliable real-time detection and identification of hazardous materials is an ongoing goal with beneficial impacts for many sectors such as health, environment, military, and defence [1–3]. The ideal platform should be operational over a wide range of deployment and environmental conditions, coupled with ease of integration, affordable, and sensitive towards several types of targeted analytes at low concentrations. A plethora of modern and conventional instrumental techniques have been successfully commercialized for ultralow concentration detection, for example, surface plasmon resonance (SPR) [4], quartz crystal microbalance (QCM) [5], mass spectrometry (MS) [6], high performance liquid chromatography (HPLC) [7], and electrochemical impedance spectroscopy (EIS) [8]. However, these techniques are generally time-consuming in data acquisition and sample preparation. Additionally, the equipment can be expensive to run with high maintenance costs, the sampling technique is usually destructive, and there is often poor discrimination of the targets presenting common chemical functional groups. On the other hand physicochemical techniques, specifically vibrational spectroscopic methods like Fourier-transform infrared (FTIR) [9] and Raman spectroscopy [10] may provide attractive alternatives because they combine ease of operation with speedy analyses, they are noninvasive, and they provide direct access to chemical functional groups (i.e., molecular structure information).

Finally, due to the specific difference in selection rules between Raman scattering and infrared absorption, sufficient complementary information can be collected without the need for further experimentation or analyses.

The illegitimate smuggling of banned rodenticides and pesticides still constitutes a global source of potential hazards and threats to public health and safety. Individuals who are exposed to these chemicals will probably face serious health complications, even life-threatening in some cases. Therefore healthcare providers need the ability to ascertain the source of this hazard in order to provide fast, appropriate treatment. Tetramethylenedisulfotetramine (TETS) is an odourless, tasteless, white crystalline neurotoxic rodenticide [11]. Its toxicity is attributed to a noncompetitive, irreversible binding to γ-aminobutyric acid-mediated chloride channel receptors ($GABA_A$). The critical human dose for this potent poison is as little as 7.0–10.0 mg of total dose and 100 to 300 μg/kg for mammals [11], making it 100 times more toxic than potassium cyanide and a more powerful convulsant than strychnine [12]. Its continuous illicit use has caused over 14,000 cases of intoxication in China between 1999 and 2010 and more than 932 human fatalities [13]. Moreover, it persists in the environment where it remains toxic up to 6 weeks in water and tissues (secondary and tertiary poisoning scenarios are also plausible) [14], and the absence of a specific antidote makes TETS a global threat that could result in mass casualties if released accidentally or by intentional malicious acts [15].

Recently Mayer et al. [16] have shown the capability of beta-cyclodextrin (β-CD) for binding TETS through host-guest complexing with a binding constant, $K_{\text{binding}} = 537 \pm 26\,M^{-1}$, thus providing a new perspective for detection of TETS and an opportunity to engineer a more general molecular-recognition platform. Cyclodextrins, also denoted as "inclusion hosts" or "cavitand," constitute an important class of "artificial receptors" in supramolecular chemistry due to their ability to complex with various guest molecules in their hydrophobic cavities (host-guest complex interactions). They are cyclic oligosaccharides consisting of 6 (α-CD), 7 (β-CD), or 8 (γ-CD) glucose units linked by 1,4-α glucosidic bonds [17]. The main driving forces of cyclodextrins in forming complexes are hydrophobic interaction, van der Waals forces, changes in solvation energy, and hydrogen bonding. Accordingly, the guest binding depends selectively on the molecule's size, shape, and charge.

These combined facts have prompted us to explore an unconventional strategy to develop a simple yet sensitive capturing platform. In this proof-of-concept study we tested an approach which integrates supramolecular recognition functionality to plasmonic substrates to increase their detection capability. The surface of the substrates is decorated with β-CD for specific capture and direct identification of TETS through its vibrational spectroscopic signature.

2. Materials and Methods

All the chemicals and solvents used below were of reagent grade and purchased from Sigma-Aldrich. They were used as-received without further purification unless otherwise indicated.

2.1. Synthesis of 6^A-O-p-toluenesulfonyl-β-cyclodextrin (β-CD-OTs) [18]. 10.0 g (8.8 mmol) of β-cyclodextrin (dried overnight under vacuum at 100°C) was dissolved in 225 mL of distilled water at 60°C under vigorous stirring until it dissolved completely. As soon as the milky solution cooled to room temperature, 7.83 g (35.25 mmol) of powdered 1-(p-toluenesulfonyl) imidazole was added and stirred for 2 hours. 4.5 g of sodium hydroxide (NaOH) dissolved in 12.5 mL of distilled water was added subsequently over 20 minutes. Unreacted 1-(p-toluenesulfonyl) imidazole was separated by filtration and the reaction was quenched by addition of 12.05 g (0.225 mol) of ammonium chloride (NH_4Cl) with continuous stirring in order to dissolve all solids. The mixture was then concentrated to almost half its volume when the product began to precipitate out. The suspension was filtered and the collected white powder was washed with excess acetone and dried in a desiccator until a constant weight over P_2O_5 to yield 4.0 g (40%). The product was confirmed by MALDI-TOF (positive ion mode); an ion of m/z 1311.20 [M+Na^+] was detected. ^{1}H NMR (500 MHz, DMSO-d_6): δ_H (ppm) = 2.43 (3H, s), 3.20–3.66 (40H, m, overlap with HDO), 4.15–4.25 (1H, m), 4.30–4.37 (m, 2H), 4.44–5.57 (2H, m), 4.76 (2H, br s), 4.82 (4H, br s), 5.61–5.82 (14H, m), 7.42 (2H, d, J = 8.2 Hz), 7.74 (2H, d, J = 8.2 Hz); ^{13}C (125 MHz, DMSO-d_6): δ_c (ppm) = 21.17, 59.3–59.9 (m), 68.9, 69.7, 72.0–73.05 (m), 80.7–81.4 (m), 101.2–102.2 (m), 127.5, 129.8, 136.7, 144.7 (see Scheme 1).

2.2. Synthesis of Mono (6-deoxy-6-mercapto)-β-cyclodextrin (β-CD-SH) [19–21]. A solution of 6^A -O-p-toluenesulfonyl-β-cyclodextrin (4.0 g, 3.11 mmol) and thiourea (4.0 g, 52.56 mmol) in 200 mL 80% methanol-water (v/v) was brought to reflux for 48 hours. The solvent was then removed in a rotary evaporator under vacuum and the white powder residue was treated with 60 mL of methanol with continuous stirring with the precipitate (isothiouronium salt) filtered and washed with plenty of acetone. The air-dried powder was dissolved in a solution of sodium disulfite (0.028 g, 0.146 mmol) in aqueous 1 M NaOH (25 mL) with stirring for 30 minutes at room temperature, then acidified with 1 M HCl to pH 3 followed by the addition of trichloroethylene (1.5 mL), and the resulting mixture was sonicated for 10 minutes. The resulting precipitate was filtered, recrystallized from ice-cold water, and dried to a constant weight as a white fine powder (1.26 g, 31.5% yield). The product was confirmed by MALDI-TOF (positive ion mode), an ion of m/z 1173.30 [M+Na^+] was detected. The presence of thiol (–SH) functional group was confirmed by the Raman vibration signature [22] at 2586 cm^{-1} (Figure S1 in ESI; see Supplementary Material available at http://dx.doi.org/10.1155/2014/207258). ^{1}H NMR (500 MHz, DMSO-d_6): δ_H (ppm) = 2.06 (SH, t, J = 7.7 Hz), 2.76 (1H, m), 2.98 (1H, m), 3.27–3.41 (14H, m, overlap with HDO), 3.40–3.81 (26H, m), 4.40–4.95 (m), 4.4–4.52 (6H, m), 4.83, 5.59–5.85 (14H, m); ^{13}C (125 MHz, DMSO-d_6): δ_c

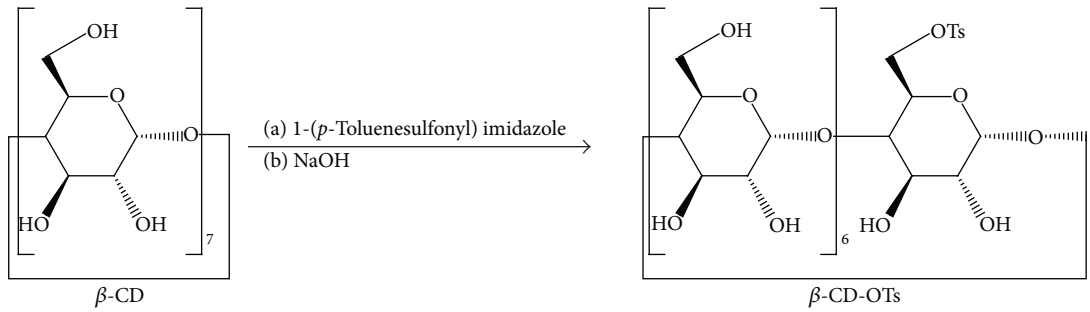

Scheme 1: Synthesis of toluenesulfonyl-β-cyclodextrin.

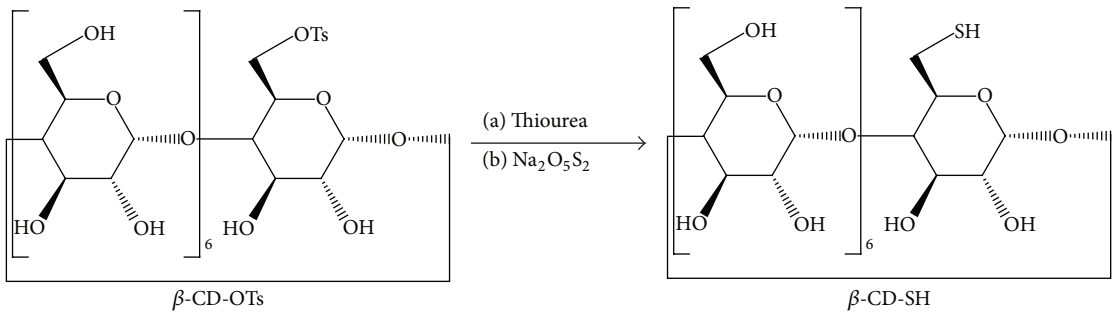

Scheme 2: Synthesis of mono-thiol-β-cyclodextrin.

(ppm) = 25.6, 59.9, 71.1, 72, 72.4, 73, 81.5, 81.7, 84.05, 101.9, 102.2 (see Scheme 2).

2.3. Synthesis of Tetramethylenedisulfotetramine (TETS) [23]. A solution consisting of 1,3,5-trioxane (0.72 g, 8 mmol) and sulfamide (1.16 g, 12 mmol) in 30 mL trifluoroacetic acid was stirred at 0°C for 3 hours and then left overnight at room temperature under continuous stirring. The solution was then cooled in an ice bath and 20 mL of distilled water was added, resulting in a white fine precipitate (1.28 g) that was collected by filtration and air-dried. The powder was redissolved in a minimum amount of ultrapure acetone and reprecipitated by slowly adding hexane and the product was dried overnight in air (1.09 g). ^{1}H NMR (500 MHz, DMSO-d_6): δ_H (ppm) = TETS 5.55 (8H, s); HEXS 5.22 and 5.59 (12H, d, J = 15.3 Hz); ^{13}C (125 MHz, DMSO-d_6): δ_c (ppm) = 70.84 (TETS); 60.83 (HEXS). Analysis of the reaction product by ^{1}H NMR yields a product distribution of 66.7% TETS and 33.3% HEXS (hexamethylenetrisulfohexamine,a side product). We did not detect the presence of sulfamide in NMR. No attempt has been made to separate them and herein we refer the titled compound as TETS/HEXS unless otherwise specified (see Scheme 3).

2.4. Gold Colloid Synthesis. Solutions containing 10 nm gold nanoparticle were prepared by reduction of hydrogen tetrachloroaurate (III) trihydrate ($HAuCl_4 \cdot 3H_2O$) using trisodium citrate ($Na_3C_6H_5O_7$) according to the protocol of Sutherland and Winefordner with slight modification [24]. In this method two stock solutions (A and B) were prepared and heated separately then mixed together at 60°C (solution A: 1 mL of 1 wt.% aqueous $HAuCl_4$ dissolved in 80 mL Milli-Q water; solution B: 4 mL of 1 wt.% tri-sodium citrate mixed with 16 mL of Milli-Q water and 0.08 μL of tannic acid). The mixing process resulted in a noticeable color change. The final solution was dark black and turned into dark red as the temperature reached 95°C indicating the end of the synthesis. All glassware were immersed and cleaned in Standard Clean 1 solution (1 : 1 : 5 volume ratio of NH_4OH (25 wt.% solution) : H_2O_2 (30 wt.% solution) : H_2O_2) for at least 10 minutes at 85°C to reduce contamination and remove all sources of ion that might affect the final size distribution and properties of the colloidal gold solutions.

2.5. Nanoparticle Immobilization [25]. The colloidal gold solution was centrifuged (single cycle) at 15000 RPM for 45 minutes to remove excess ions, which include sodium, citrate, and tannates, and the gold nanoparticles were concentrated by dissolving them in 10 mM of citrate buffer at pH 4.0 (the volume of the buffer solution was 4 times less than the volume of the original centrifuged solution). A thin film of Au (~200 nm) with a Ti under-layer (~50 nm) on silicon substrates was first washed for 20 minutes in Standard Clean 1 solution to remove all contaminants from the fabrication process and directly immersed into a 2 mM 1,8-octanedithiol in ethanol solution for 24 hours. They were then reacted for 2 hours with 20 mM DL-dithiothreitol in Tris-HCl (50 mM)/EDTA (5 mM), a step required in order to achieve a reduced uniform thiol layer, and afterward rinsed thoroughly with Milli-Q water and immersed in the concentrated gold colloidal solution described above for 2 hours. At this particular ionic strength of the buffer solution,

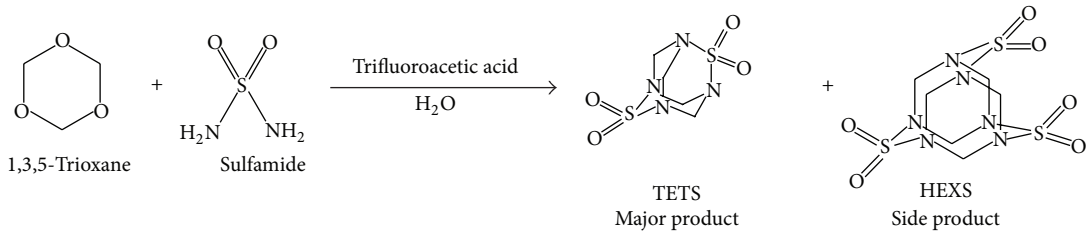

Scheme 3: Synthesis of TETS.

we expect the gold nanoparticles to self-assemble with an estimated surface coverage of 30% (refer to Figure S2 in the electronic supplementary information (ESI) for scanning electron microscopy (SEM) photomicrographs).

2.6. CD Immobilization and Complexation. Stand-alone, unmounted Klarite (KLA 313) substrates were purchased from Renishaw Diagnostics and used as received. The SERS-active surface is composed of regular arrays of gold-coated textured silicon comprising inverted pyramid structures (~1.5 μm wide and 1 μm depth), (SEM photomicrographs of the surface are shown in ESI Figure S3). The Klarite substrates were incubated in 10 mM deoxygenated solution of mono-thiol-β-CD (DMSO/H_2O) [26] for 30 hours in the dark (nitrogen gas was bubbled into the solution to remove oxygen). Afterwards the substrate was washed consecutively with DMSO and water in order to remove noncovalently bonded CD molecules and impurities, dried under a stream of argon gas flow then subsequently immersed for another 30 hours in 1 mM reagent-grade acetone solution of TETS/HEXS. The substrates were then rinsed with acetone and dried gently with a stream of argon gas before microscopic and spectroscopic measurements. The same procedures have been employed for our home-made Au NPs-decorated substrates. All samples were stored in a vacuum desiccator and transported in argon-gas filled containers to minimise contamination from the surrounding atmosphere.

2.7. Raman. Raman spectra for the detection of CD and TETS/HEXS vibrational bands were collected using a Jobin-Yvon LabRam Raman spectrometer (backscattering configuration) equipped with a 300 L/mm grating (resolution 2.2 cm^{-1} at 633 nm). HeNe laser excitation beam (633 nm) was focused on the substrate surface with long working distance ×100 (N.A 0.6) and ×20 (N.A 0.35) microscope objectives, at 10 sec integration time (unless stated otherwise) and with 2.5 mW intensity. All spectra acquisition was carried out after the grating position of the spectrometer was calibrated against the Si (100) phonon mode at 520 cm^{-1}.

2.8. X-Ray Photoelectron Spectroscopy (XPS). XPS was undertaken on a Kratos Axis UltraDLD surface analyzing chamber using the K_α line of monochromatised Al (1486.6 eV) as the radiation source to determine the chemical functionality and concentration of CD and TETS/HEXS on the surface. A power of 150 W was used in conjunction with detector pass energy of 160 eV for the survey scans and 20 eV for the core-level narrow-scans. Sample charging was accounted for by shifting all the XPS peaks to fix the Au $4f_{7/2}$ peak at 84.0 eV binding energy [27]. Fitting to the spectra was performed using a combination of Gaussian and Lorentzian components, and the asymmetry parameter may be varied from 0 to 50 %. The XPS survey scans did not detect the presence of impurities such as Cl and Na coming from the chemical syntheses, plus the aromatic hydrocarbon signatures (e.g., from toluenesulfonyl) are absent in both XPS and vibrational spectroscopy. This confirms that we have negligible contaminants on our surfaces under study and they do not influence our results presented below.

2.9. Attenuated Total Reflectance Fourier-Transform Infrared (ATR-FTIR). ATR-FTIR spectra for detecting the infrared vibrational bands of CD and TETS/HEXS were collected using a Perkin Elmer Spectrum One FT-IR spectrometer with an universal triple bounce ATR sampling accessory (diamond/ZnSe composite crystal), using a spectral resolution of 4 cm^{-1}, averaging over a minimum of 36 scans and until the intensity of the most intense band does not change by more than 5%. A helium-neon laser operating at a wavelength of 633 nm was used as the excitation source over a sampling area of 16 mm diameter. All ATR-FTIR spectra were recorded in the absorbance mode.

2.10. DFT Calculation. Vibrational spectra calculations for TETS and HEXS were performed with the Gaussian 09 software package using density functional theory (DFT) methods with the B3LYP [28] hybrid exchange-correlation functional and the 6-311++G(d,p) basis set. The Raman scattering cross-sections, $d\sigma/d\Omega$, at room temperature were calculated according to the equation [29] below:

$$\begin{aligned}\frac{d\sigma}{d\Omega}\left(\mathrm{cm}^2 \times \mathrm{sr}^{-1}\right) &= 5.8 \times 10^{-46} \times \frac{\left[10^7/\left(\lambda_{l(\mathrm{nm})} - k(\mathrm{cm}^{-1})\right)\right]^4}{k(\mathrm{cm}^{-1})} \\ &\times L_M \times \left(R_k\left[\text{Å}^4/\mathrm{amu}\right]\right) \\ &\times \left(1 - \exp\left(\frac{-k(\mathrm{cm}^{-1})}{201.56}\right)\right)^{-1},\end{aligned} \quad (1)$$

where λ_L is the wavelength of the laser; $_k$ is the wavenumber of the vibrational mode; L_M is the local field correction, which depends on the index of refraction of the environment (taken here as 1); and R_k is the Raman activity.

3. Results and Discussion

3.1. Raman Spectroscopy. Raman bands due to organic moiety are noticeable just below 3000 cm^{-1} (Figure 1) on the various treated surfaces of the Klarite substrate. However, due to the low Raman scattering intensities and low signal-to-noise ratio, it is difficult to identify Raman bands of either mono-thiol-β-CD or TETS/HEXS inclusion in these spectra (Figures 1(iii) and (v)). Evidence indicating the successful immobilization of the β-CD on the substrate and the inclusion of TETS/HEXS into CD is presented in the XPS section. Based on the magnitude of the signal intensity, no surface-enhanced Raman scattering was observed from either the mono-thiol-β-CD immobilized on Klarite or the inclusion complex, TETS/HEXS (Figures 1(iii) and (v)). The rated average enhancement of the Klarite gold substrate is in the order of 10^6 [30], but this factor alone does not guarantee enhancement to the Raman signal. Other important factors to consider are (i) the distribution and concentration of the sites providing the highest enhancement factor, and the affinity of the molecules to these sites; (ii) the concentration and surface distribution of the molecules; and (iii) the intrinsic Raman scattering properties of the inclusion molecules. Since we are using commercial SERS-active substrates, we will not consider factor (i) as this is optimized by the manufacturer and we are not altering the physical nature of the substrate other than self-assembling CD on them.

To investigate the Raman scattering properties of the inclusion molecules in greater detail, we first performed DFT vibrational calculations on TETS and HEXS (Tables S1 and S2 in ESI list all simulated modes and cross-section calculation details) in order to estimate their intrinsic differential Raman cross sections ($d\sigma/d\Omega$) and compare with those of a dye molecule commonly used in SERS experiments, Rhodamine 6G (R6G), at the same excitation wavelength (633 nm). As shown in Figure 2, TETS/HEXS exhibited weak differential cross-section values ($<10^{-29}$ cm^2/sr). These values are low, even less than those of many nonresonant molecules, which are in the order of 10^{-29} to 10^{-30} cm^2/sr [31]. On the other hand, R6G at preresonance condition exhibits $d\sigma/d\Omega$ values of 10^3 to 10^4 fold higher (Figure 2, 633 nm trace) than TETS/HEXS, and as high as 10^7-fold at resonance condition (Figure 2, 532 nm trace) [32, 33]. The latter highlights the importance of selecting the correct excitation wavelength to observe enhancement originating from electronic transitions.

Another contributing factor to the negligible Raman intensity from TETS/HEXS is their relatively low surface concentration (~28 pmol/cm^2) which is caused by the discontinuous distribution of β-CD across the surface together with a TETS/HEXS to CD ratio of ~1/6 (refer to the XPS section below for details). This is further demonstrated by a drop-cast experiment where it was not until the third drop, an equivalent of 18.8 nmol/cm^2 (each drop had a volume of 10 μL containing 1 mM of TETS/HEXS dissolved in acetone and allowed to dry over the Klarite SERS-active area (0.16 cm^2) before Raman measurement), that a few Raman bands could be observed (Figure 1(iv)). The combined low Raman scattering cross section at 633 nm and a low surface coverage of TETS/HEXS is the most likely explanation for their unsuccessful detection with Raman.

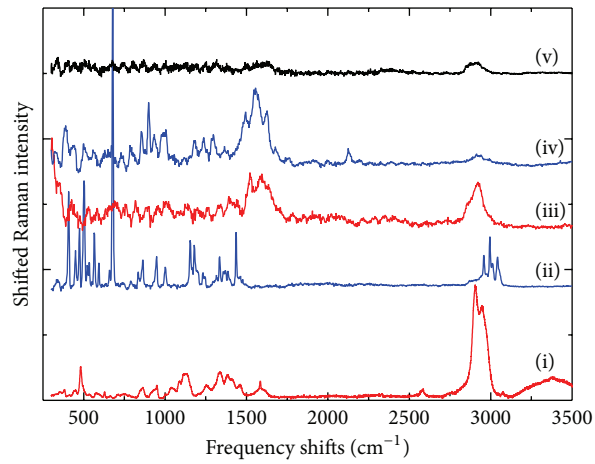

Figure 1: We have demonstrated a supramolecular platform for detection of selective inclusion molecules by vibrational spectroscopy. Our experimental data show that functionalizing commercial Klarite SERS substrates with β-CD as a molecular receptor for TETS/HEXS was not effective for Raman spectroscopic detection, most likely due to the extremely weak differential cross section of these molecules at 633 nm excitation wavelength coupled with its relatively low surface concentration and discontinuous distribution on the surface. XPS confirms the surface of the Klarite was decorated with mono-thiol-β-CD, but the concentration was low, around 0.07 per unit formula per Au site (or 161 pmol cm^{-2}) on the SERS-active area. Furthermore, the TETS/HEXS to CD ratio indicates only 1 in every 6.25 CD cavities is occupied by TETS/HEXS. On the other hand, we found that ATR-FTIR is able to detect these molecules most successfully when the surface is decorated with Au NPs. The NPs increase the number of self-assembled mono-thiol-β-CD molecules per unit area, giving a higher surface concentration of TETS/HEXS per unit measurement area for infrared detection. ATR-FTIR coupled with a NP-functionalized surface is therefore a viable alternative vibrational-based detection platform, as the absorption cross section of the molecules is always inherently much greater than the Raman scattering cross section. Comparison of the raw Raman spectra from powder sample of mono-thiol-β-CD (i) and TETS/HEXS (ii), those of mono-thiol-β-CD (self-assembled from 10 mM solution) on SERS-active Klarite surface (iii), drop-casted TETS/HEXS solution (6 sec integration time) on SERS-active Klarite surface (iv), and TETS/HEXS inclusion in mono-thiol-β-CD decorated SERS-active area of the Klarite surface (v).

3.2. X-Ray Photoelectron Spectroscopy. Figure 3 shows the XPS spectra of the N 1s (Figure 3(a)) and S 2p (Figure 3(b)) regions which verify the presence of the inclusion and the attachment of CD on the Klarite surfaces. The N 1s XPS peak centered at 400.6 eV is well defined and well above the level of possible nitrogen contamination due either to adsorption from atmosphere or from sample preparation. Each of the

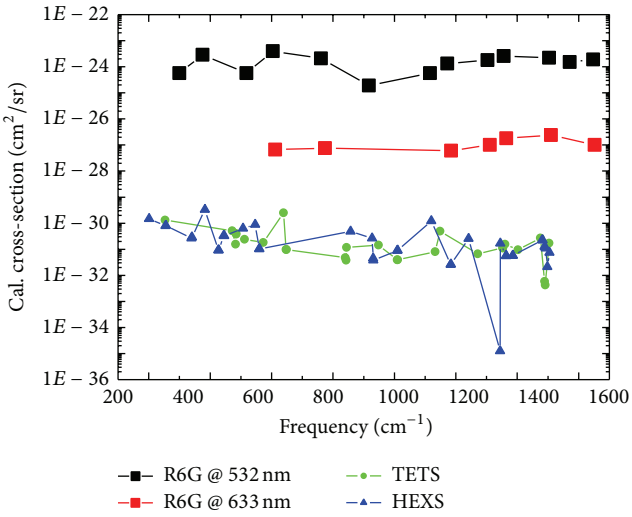

FIGURE 2: Calculated differential Raman cross-section (cm^2/sr) compared with that of R6G from the literature (at 532 nm excitation (resonant) [32] and at 633 nm laser excitation (preresonant) [33]) and those of HEXS and TETS from our work. The total cross-section values, σ (cm^2), of R6G at 532 nm from [32] were transformed into differential cross-section, $d\sigma/d\Omega$ (cm^2/sr), by the following relationship [29], $\sigma = ([(8\pi)/3) \times (1 + 2\rho)]/(1 + \rho)) \times (d\sigma/d\Omega)$, where ρ is the depolarization ratio of R6G taken as 1/3 [51].

nitrogens in TETS/HEXS are single-bonded to two $-CH_2-$ and one $-SO_2$ functional groups, hence the XPS N 1s peak should appear above that of an alkylamine [34, 35] N 1s XPS peak at 400.0 eV and below 403.0 eV attributed to that of oxidized nitrogen [36, 37] (e.g., NO_x). We can confidently assign our N 1s XPS peak to TETS/HEXS, which also are the only molecules that contain nitrogen in our self-assembling system. The S 2p XPS also shows the presence of sulfonyl species (–S=O) from TETS/HEXS centered at 168.7 eV (S $2p_{3/2}$). The amount of TETS/HEXS derived from this S 2p peak with respect to the pure Au 4f (Figure 3(c)) peak is 0.012 ± 0.004 per unit formula per Au site, which is close to the value calculated from the N 1s XPS peak at 0.017 ± 0.007 per unit formula per Au site, well within the experimental uncertainties. The other two sets of doublets in the S 2p spectrum can be assigned to bound and unbound sulfur species [38]. The set of peaks at lower binding energy, 161.8 eV (S $2p_{3/2}$) and 163.0 eV (S $2p_{1/2}$) with an intensity ratio of 2 : 1 and spin-orbit-splitting of 1.2 eV, belongs to monothiolated β-CD attached to the gold surface, that is, β-CD–S–Au, while that at the higher binding energy, 164.0 eV (S $2p_{3/2}$) and 165.2 eV (S $2p_{1/2}$), belongs to those of unbound β-CD–SH. The former is also evident as a small deconvoluted peak at 1.1 eV higher in binding energy compared with that of the pure Au 4f peak (Au $4f_{7/2}$ at 84.0 eV), which can be assigned to Au–S (Figure 3(c)) [39]. The presence of unbound β-CD–SH molecules is not unusual and has been identified in several studies, and is verified by our own XPS measurement of thiolated β-CD powder (Figure S4 in ESI). According to the investigation of saturation times of CD–SH on Au surfaces by Velic et al. [40] and Weisser et al. [41], stable multilayers of CD–SH (both bound and unbound) are present even after a short time (for only 5 minutes) after immersing Au surfaces in 100 μmol/L of CD–SH solution with rinsing during or after the self-assembling process. We also found the ratio of bound and unbound mono-thiol-CD is quite similar on both surfaces, which implies that the Au binding sites are similar on both surfaces, as indicated by the X-ray diffraction (XRD) analysis below.

The C 1s XPS spectrum of the self-assembled CD with TETS/HEXS inclusion on the SERS-active Au surface is shown in Figure 3(d). The spectrum can be well fitted with three peaks as hydrocarbon (C–H/C–C) at 284.9(0) eV, alcohol/ether/thiol (C–O/C–O–C/C–S) at 286.8(9) eV, and acetal/diamine (O–C–O/N–C–N) at 288.2(4) eV binding energy. This is consistent with the increase in binding energy relative to hydrocarbon of each oxygen bond with carbon of 1.6 eV with the contribution from nitrogen containing species increasing the uncertainty to greater than ± 0.1 eV [38, 39]. Quantitative analysis of the XPS C 1s signal after subtracting the contribution from TETS/HEXS gives a CD coverage of 0.07 ± 0.03 per unit formula per Au site on the SERS-active area, while that on the flat Au area is much lower at 0.03 ± 0.02 per unit formula per Au site. Our XRD measurements show a (111) configuration of the gold atoms on the flat Au surface, while the SERS-active gold region shows a predominantly (111) diffraction pattern plus other minor (*hkl*) reflections (Figure S5 in ESI) as expected due to the geometry of the nanoengineered surface. Assuming there are 1.39×10^{15} Au atoms per cm^2 for a single atomic layer of close-packed Au [40], the surface coverage of CD on the SERS area is estimated to be 9.7×10^{13} molecules per cm^2 and that on the flat surface is 4.2×10^{13} molecules per cm^2. The latter is similar to those reported in the literature for mono-thiol-β-CD [40] and per-thiol-β-CD [42]. Despite this low CD coverage on the Au surfaces, we found the number of the inclusion molecule to CD ratio to be the same in both surfaces, which is around 16 ± 5%, indicating the TETS/HEXS molecules are complexed to CD and, as expected, independent of surface adsorption sites. For the case where TETS/HEXS are adsorbed onto the intermolecular vacancies, the nanoengineered SERS gold surfaces, which have a larger surface area, should show a higher number of TETS/HEXS per CD ratio. The inclusion of ferrocene into per-thiol-β-CD anchored on a gold surface shows that only half of the CD cavities are occupied by ferrocene or an equivalent of 25 pmol cm^{-2} [26]. Our study also confirms the fact that not all of the CD cavities are occupied, which is equivalent to 28 pmol cm^{-2} (of 161 pmol cm^{-2} of mono-thiol-β-CD) and 11 pmol cm^2 (of 70 pmol cm^{-2} of mono-thiol-β-CD) of TETS/HEXS presence on the SERS-active and flat Au surface, respectively.

3.3. Attenuated Total Reflectance FTIR. Figures 4(a) (iii) and (iv) show the attenuated total reflectance Fourier-transform infrared (ATR-FTIR) spectra of TETS/HEXS CD inclusion complex on the Klarite surfaces. We were able to detect vibrational bands from 1020 to 1135 cm^{-1} originating from the various stretching and bending modes of (C–C/C–O), which are attributed to the immobilized mono-thiol-β-CD [43]. Comparing with the ATR-FTIR spectrum of unbound

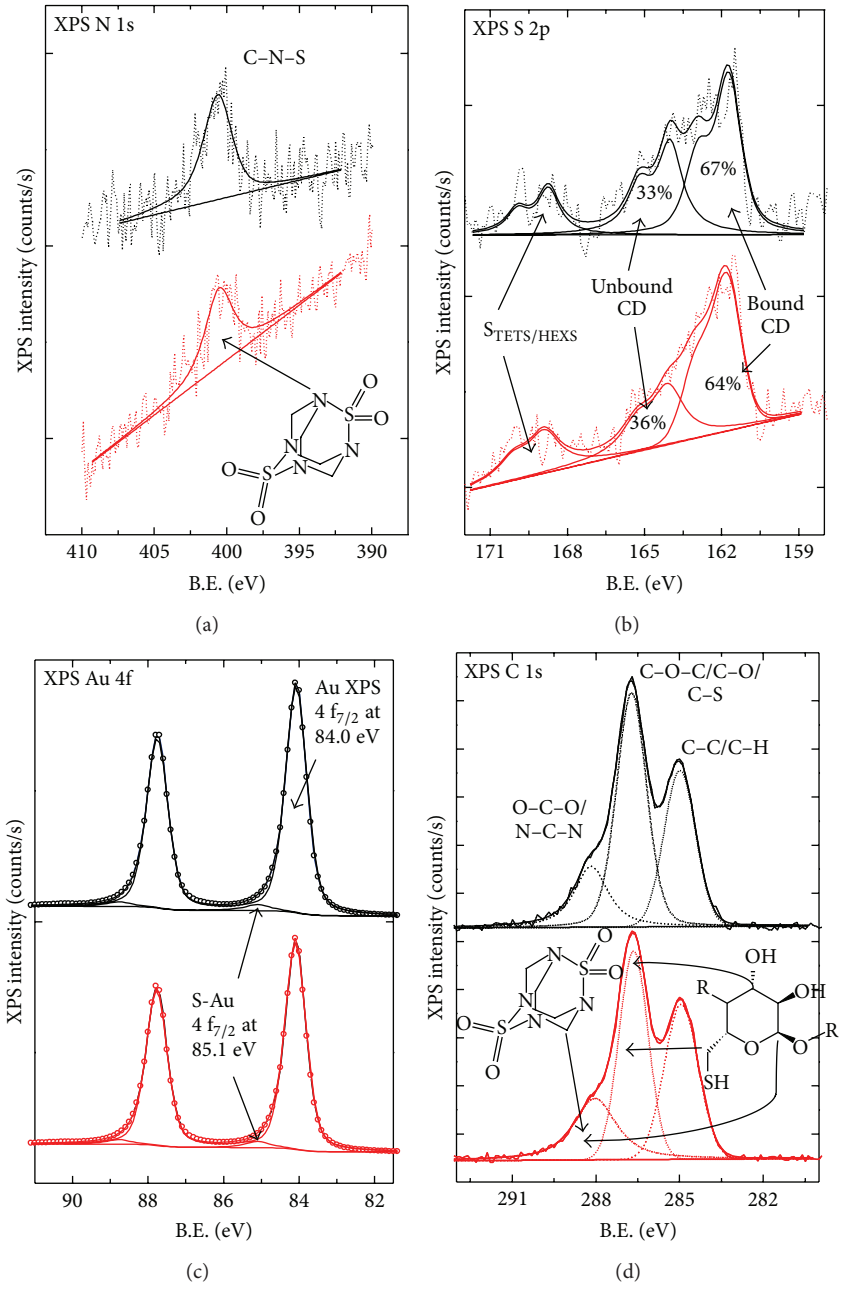

FIGURE 3: Core-level XPS of N 1s (a), S 2p (b), Au 4f (c), and C 1s (d) of the TETS/HEXS CD inclusion complex on the different surfaces of a Klarite substrate. On each of the core-level spectra, the top (black) curve is taken from the SERS-active area and the bottom (red) curve is from the non-SERS-active flat Au surface. The molecule shown in (a) is that of TETS and the thiolated portion of a β-CD molecule is shown in (d). The arrows indicate the functional groups that are responsible for the observed XPS core-level peaks.

mono-thiol-β-CD powder (Figure 4(a) (i)) these bands are shifted to higher wavenumbers, which is also previously observed on mono- and multithiolated CD attached on Au surfaces as compared to the IR spectra taken by the KBr method [44]. According to Nelles et al. [44] this is due to the change in degree of ordering among the cyclodextrins when they are immobilized on the gold surface. Furthermore, the authors also found that the antisymmetric glycosidic ν_a(C–O–C) vibration band at 1155 cm^{-1} for all the cyclodextrin derivatives investigated in their study do not shift in the KBr and immobilized CD film spectra. We have also found the ν_a(C–O–C) vibration in our immobilized mono-thiol-β-CD sample appearing at almost the same position as those in the unbound CD powder. Another characteristic vibrational band related to the cyclodextrin ring vibration is the skeletal mode of β-CD involving the α-1,4 linkage at 944 cm^{-1} [43–45], which also remains unshifted compared with the powder spectrum.

Having said this, both the 1155 and 944 cm^{-1} vibrational bands from the CDs are positioned very close to two intense

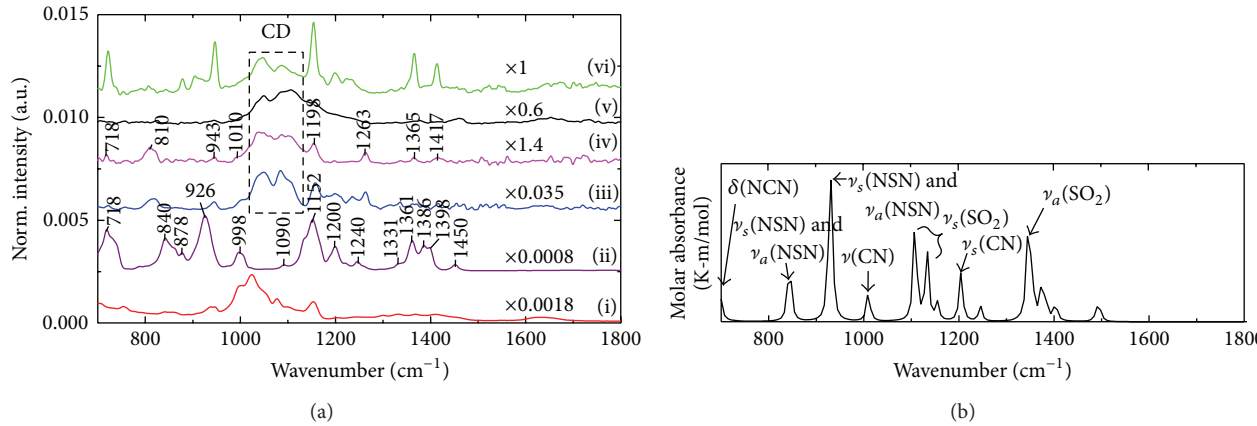

FIGURE 4: (a) ATR-FTIR spectra of mono-thiol-β-CD powder (i), as-synthesized TETS/HEXS powder (ii), TETS/HEXS inclusion in mono-thiol-β-CD decorated SERS-active area (iii), TETS/HEXS inclusion in mono-thiol-β-CD decorated flat Au Klarite surface (iv), mono-thiol-β-CD decorated Au nanoparticles anchored on a flat Au surface (v), and surface in (v) after incubated in TETS/HEXS solution (vi). The spectra are normalized for comparison. (b) Sum of the individual calculated IR vibrational spectra of HEXS and TETS. ($\nu \equiv$ stretching mode; $\delta \equiv$ bending mode; subscript $s \equiv$ symmetric vibration; and subscript $a \equiv$ antisymmetric vibration).

and broad infrared vibrational bands for TETS/HEXS (powder spectrum, Figure 4(a) (ii) at 1151 and 926 cm^{-1}) most likely to be the sulfonyl, O=S=O, symmetric stretching, and N–S–N antisymmetric (higher wavenumber) and symmetric stretching modes, respectively. These assignments are based on sulfamide ($(H_2N)_2SO_2$) [46], with a similar molecular configuration. To the best of our knowledge, there are no vibrational spectroscopic studies of TETS or HEXS in the literature; hence, we have also carried out DFT calculations on TETS and HEXS to investigate their infrared vibrational modes (refer to Tables S1 and S2 in ESI for a full list of harmonics and their corresponding IR intensities). Figure 4(b) is plotted to compare the calculated (sum of the simulated individual TETS and HEXS spectra) and the experimental room-temperature absorption spectrum of Figure 4(a) (ii). We found good agreement of the band positions between the calculated and experimental vibrational modes, despite that the maximum intensities of some bands do not appear at the same position, for example, the vibrational bands between 1100 and 1180 cm^{-1}. Also, several bands are unaccounted in the calculated spectrum, especially in the region of 700 to 800 cm^{-1}. A thorough assignment of all the vibrational bands will be the subject of further work. At this stage we will focus on several important vibrational bands and base our assignment of the TETS/HEXS vibrational bands on those of sulfamide [46] and hexamethylenetetramine [47, 48] as reported in the literature. A tentative assignment of the major vibrational bands is listed in Table 1.

Returning to the ATR-FTIR spectra of the SERS and flat Au areas of the Klarite surface, there are IR vibrational bands that can be assigned to TETS/HEXS which do not coincide with any vibrational bands (or weak in intensity) from the immobilized CD. The weak to medium vibrational bands from 1200 to 1264 cm^{-1} can be assigned to C–N stretching and CH_2 rocking from TETS/HEXS, and the shoulder at 1010 cm^{-1} on both spectra is most likely due to a fundamental C–N stretching mode of the ring vibration. These two C–N stretching modes are essentially the fingerprint vibrations for the hexamethylenetetramine (Hmta) derivative cage molecules [48]. There is also a medium vibrational band at 810–817 cm^{-1}, which coincides with vibrational bands from neither TETS/HEXS nor CD. In fact, none of these latter IR bands appear in the ATR-FTIR spectrum of the mono-thiol-β-CD decorated Au nanoparticles immobilized onto a flat Au surface without any inclusion molecules (Figure 4(a) (v)). Despite the low infrared signal coming from the inclusion molecules, changes to the shape and position of the TETS/HEXS and CD absorbance bands plus the emergence of new vibrational bands imply ATR-FTIR was able to detect the minute amount of TETS/HEXS inclusion in mono-thiol-β-CD. As indicated from XPS the concentrations of the inclusion molecule and CD are very small; thus, the introduction of nanoparticles (NPs) should increase the number of Au adsorption sites through an increase in surface area per unit area. This in principle should increase the density of immobilized mono-thiol-β-CD per unit area with a concurrent proportional increase of the inclusion molecules thus improving the detection (and signal-to-noise ratio) of TETS/HEXS by ATR-FTIR. The 10 nm Au NPs chosen in this study is merely for their ease of preparation in our laboratory and not for their SERS activity, which they should not be in this particle size range and their nonuniform surface distribution [49].

Figure 4(a) (vi) shows the ATR-FTIR spectrum of mono-thiol-β-CD immobilized on Au nanoparticles (NPs) decorated flat Au surface after incubation for the same period of time and in a TETS/HEXS solution with the same concentration as the Klarite surfaces used in the Raman and XPS study. As well as the observation of vibrational bands due to mono-thiol-β-CD at 1045 and 1086 cm^{-1}, we also observed very sharp and intense bands at 722, 946, 1154, 1366, and 1414 cm^{-1}, plus weaker vibrational bands from 800 to 905 cm^{-1} and 1180 to 1300 cm^{-1}. These are not observed in Figure 4(a) (v) for the bare CD decorated Au NP substrate. Almost all of these

Table 1: Observed frequencies and tentative band assignments of major peak in ATR-FTIR spectrum of TETS/HEXS inclusion in mono-thiol-β-CD anchored on 10 nm Au NPs immobilized on a gold surface (Figure 4(a) (vi)).

Experimental frequency (cm^{-1})	Assignments		Calculated frequency (cm^{-1})[c]
	CD[a]	TETS/HEXS[b]	
1414 s	Φ OCH, Φ CCH (1415 cm^{-1} m)	CH_2 twist, wag (1386–1400 cm^{-1} s)	1400 wm
1366 vs	Φ CCH, Φ OCH, Φ COH (1365 cm^{-1} m)	SO_2 antisym. stretching (1361 cm^{-1} s)	1344 vs
1233–1223 m		CH_2 rocking (1246 cm^{-1} w)	1240 wm
1198 m	r CO, Φ CCH, Φ COH (1197 cm^{-1} w)	CN stretching (1199 cm^{-1} m)	1204 s
1154 vs	r CO, r CC, Φ COH, Φ COC (1155 cm^{-1} s)	SO_2 sym. stretching (1151 cm^{-1} vs)	1155 wm, 1134 vs, 1106 vs
1086 s, broad	r CO, Φ COH, r CC (1087–1102 cm^{-1} vs)		
1045 vs, broad	r CC, Φ COH, Φ CCH, Φ CCO, r CC (1014–1051 cm^{-1} vs)		
1006 m, shoulder		CN stretching (1000 cm^{-1} m)	1008 m
946 vs 904 m	Skeletal vib. α-1,4 linkage (945 cm^{-1} s)	NSN antisym. and sym. stretching (904–931 cm^{-1} vs, broad)[d]	931 vs
879 m	Φ CCH, r CO, r CC (849 cm^{-1} m)	NSN antisym. and sym. stretching (842–878 cm^{-1} s, m)[d]	847 s
722 vs		NCN bend (719 cm^{-1} vs)	693 s

[a]Assignment according to the CD vibrational bands of bound CD on a gold surface based on those in reference [43].
[b]Assignment according to the TETS/HEXS vibrational bands of a powder sample based on sulfamide [46], and hexamethylenetetramine [47, 48].
[c]Vibrational bands of TETS and HEXS from Figure 4b.
[d]The antisymmetric vibrational bands are at higher wavenumbers, while the symmetric vibrational bands are at lower wavenumbers.

vibrational bands appear close to the vibrational bands of the powder TETS/HEXS. Most interesting is the sharpness of those five very intense vibrational bands (722, 946, 1154, 1366, and 1414 cm^{-1}) as compared with the broad vibration bands in the powder spectrum (a tentative assignment of these bands is listed in Table 1). This may be related to the orientation and interaction of the TETS/HEXS molecule inside the hydrophobic β-CD cavity. Comparing Figures 4(a) (vi) to (iii) and (iv), we found that the former has a much better signal-to-noise ratio and the inclusion and CD vibrational bands are sharper and well defined than the surfaces without the Au NPs. However, we did not detect any Raman scattering signals from CD nor TETS/HEXS on the Au NPs decorated surface since it contains no SERS active sites as mentioned above.

These findings, as supported by the NMR work by Mayer et al. on the binding of TETS to CD which shows noticeable ^{1}H NMR chemical shift for the TETS protons [16], strongly confirm the formation of the inclusion complex between TETS/HEXS and the immobilized mono-thiol-β-CD, and most important is the feasibility of our Au nanoparticle platform in conjunction with ATR-FTIR to capture and detect the neurotoxin. With further modification and optimization of both the experimental procedure (e.g., dynamic versus equilibrium incubation of TETS/HEXS into CD) and the substrate preparation (such as controlling the steric conformation of the thiolated CDs through the use of thiol-spacers [26, 42] and obtaining a uniform distribution of the Au NPs), we believe a CD on Au NPs surface platform coupled to ATR-FTIR has great potential to be used in detecting very low concentrations of targeted neurotoxins and polycyclic aromatic hydrocarbons (PAHs). Further investigations will also need to be carried out to determine the possibility of surface-enhanced IR effect on the Au NPs decorated surface [50].

4. Conclusions

We have demonstrated a supramolecular platform for detection of selective inclusion molecules by vibrational spectroscopy. Our experimental data show that functionalizing commercial Klarite SERS substrates with β-CD as a molecular receptor for TETS/HEXS was not effective for Raman spectroscopic detection, most likely due to the extremely weak differential cross section of these molecules at 633 nm excitation wavelength coupled with its relatively low surface concentration and discontinuous distribution on the surface. XPS confirms the surface of the Klarite was decorated with mono-thiol-β-CD, but the concentration was low, around 0.07 per unit formula per Au site (or 161 pmol cm^{-2}) on the SERS-active area. Furthermore, the TETS/HEXS to CD ratio indicates only 1 in every 6.25 CD cavities is occupied by TETS/HEXS. On the other hand, we found that ATR-FTIR is able to detect these molecules most successfully when the surface is decorated with Au NPs. The NPs increase the number of self-assembled mono-thiol-β-CD molecules per unit area, giving a higher surface concentration of TETS/HEXS per unit measurement area for infrared detection. ATR-FTIR coupled with a NP-functionalized surface is therefore a viable alternative vibrational-based detection platform, as

the absorption cross section of the molecules is always inherently much greater than the Raman scattering cross section.

Conflict of Interests

The authors declare that there is no conflict of interests regarding the publication of this paper.

Acknowledgments

This work is supported by the Marsden Fund of New Zealand (IRL1001) and The MacDiarmid Institute for Advanced Materials and Nanotechnology. The authors would like to thank Geoff Willmott (The University of Auckland) and Eric Le Ru (Victoria University of Wellington) for many useful discussions.

References

[1] P. A. Serra, Ed., *Biosensors For Health, Environment and Biosecurity*, InTech, Rijeka, Croatia, 2011.

[2] M. H. Erhard, R. Kuhlmann, L. Szinicz, and U. Losch, "Detection of the organophosphorus nerve agent soman by an ELISA using monoclonal antibodies," *Archives of Toxicology*, vol. 64, no. 7, pp. 580–585, 1990.

[3] J. J. Gooding, "Biosensor technology for detecting biological warfare agents: recent progress and future trends," *Analytica Chimica Acta*, vol. 559, no. 2, pp. 137–151, 2006.

[4] J. Homola, "Surface plasmon resonance sensors for detection of chemical and biological species," *Chemical Reviews*, vol. 108, no. 2, pp. 462–493, 2008.

[5] K. A. Marx, "Quartz crystal microbalance: a useful tool for studying thin polymer films and complex biomolecular systems at the solution-surface interface," *Biomacromolecules*, vol. 4, no. 5, pp. 1099–1120, 2003.

[6] A. El-Aneed, A. Cohen, and J. Banoub, "Mass spectrometry, review of the basics: electrospray, MALDI, and commonly used mass analyzers," *Applied Spectroscopy Reviews*, vol. 44, no. 3, pp. 210–230, 2009.

[7] K. Valkó, "Application of high-performance liquid chromatography based measurements of lipophilicity to model biological distribution," *Journal of Chromatography A*, vol. 1037, no. 1-2, pp. 299–310, 2004.

[8] F. Lisdat and D. Schäfer, "The use of electrochemical impedance spectroscopy for biosensing," *Analytical and Bioanalytical Chemistry*, vol. 391, no. 5, pp. 1555–1567, 2008.

[9] Z. Movasaghi, S. Rehman, and I. U. Rehman, "Fourier transform infrared (FTIR) spectroscopy of biological tissues," *Applied Spectroscopy Reviews*, vol. 43, no. 2, pp. 134–179, 2008.

[10] N. L. Jestel, "Raman spectroscopy," in *Process Analytical Technology*, pp. 195–243, John Wiley and Sons, 2010.

[11] J. Owens, S. Hok, A. Alcaraz, and C. Koester, "Quantitative analysis of tetramethylenedisulfotetramine (tetramine) spiked into beverages by liquid chromatography-tandem mass spectrometry with validation by gas chromatography-mass spectrometry," *Journal of Agricultural and Food Chemistry*, vol. 57, no. 10, pp. 4058–4067, 2009.

[12] X. Xu, G. Song, Y. Zhu et al., "Simultaneous determination of two acute poisoning rodenticides tetramine and fluoroacetamide with a coupled column in poisoning cases," *Journal of Chromatography B: Analytical Technologies in the Biomedical and Life Sciences*, vol. 876, no. 1, pp. 103–108, 2008.

[13] J.-M. Li, J. Gan, T.-F. Zeng, J. W. Sander, and D. Zhou, "Tetramethylenedisulfotetramine intoxication presenting with de novo Status Epilepticus: a case series," *NeuroToxicology*, vol. 33, no. 2, pp. 207–211, 2012.

[14] E. Croddy, "Rat poison and food security in the People's Republic of China: focus on tetramethylene disulfotetramine (tetramine)," *Archives of Toxicology*, vol. 78, no. 1, pp. 1–6, 2004.

[15] D. A. Jett and D. T. Yeung, "The CounterACT research network: basic mechanisms and practical applications," *Proceedings of the American Thoracic Society*, vol. 7, no. 4, pp. 254–256, 2010.

[16] B. P. Mayer, R. L. F. Albo, S. Hok, and C. A. Valdez, "NMR spectroscopic investigation of inclusion complexes between cyclodextrins and the neurotoxin tetramethylenedisulfotetramine," *Magnetic Resonance in Chemistry*, vol. 50, no. 3, pp. 229–235, 2012.

[17] E. M. M. Del Valle, "Cyclodextrins and their uses: a review," *Process Biochemistry*, vol. 39, no. 9, pp. 1033–1046, 2004.

[18] H.-S. Byun, N. Zhong, and R. Bittman, "6A-O-p-toluenesulfonyl-β-cyclodextrin: (β-Cyclodextrin, 6A-(4-methylbenzenesulfonate))," *Organic Syntheses*, vol. 77, pp. 225–230, 2000.

[19] F. S. Damos, R. C. S. Luz, A. A. Sabino, M. N. Eberlin, R. A. Pilli, and L. T. Kubota, "Adsorption kinetic and properties of self-assembled monolayer based on mono(6-deoxy-6-mercapto)-β-cyclodextrin molecules," *Journal of Electroanalytical Chemistry*, vol. 601, no. 1-2, pp. 181–193, 2007.

[20] J. Wang, L. Kong, Z. Guo, J. Xu, and J. Liu, "Synthesis of novel decorated one-dimensional gold nanoparticle and its application in ultrasensitive detection of insecticide," *Journal of Materials Chemistry*, vol. 20, no. 25, pp. 5271–5279, 2010.

[21] B. Jing, X. Chen, X. Wang, Y. Zhao, and H. Qiu, "Sol-gel-sol transition of gold nanoparticle-based supramolecular hydrogels induced by cyclodextrin inclusion," *Chemical Physics and Physical Chemistry*, vol. 9, no. 2, pp. 249–252, 2008.

[22] R. Tuma, S. Vohnik, H. Li, and G. J. Thomas Jr., "Cysteine conformation and sulfhydryl interactions in proteins and viruses. 3: quantitative measurement of the Raman S–H band intensity and frequency," *Biophysical Journal*, vol. 65, no. 3, pp. 1066–1072, 1993.

[23] T. Esser, A. E. Karu, R. F. Toia, and J. E. Casida, "Recognition of tetramethylenedisulfotetramine and related sulfamides by the brain GABA-gated chloride channel and a cyclodiene-sensitive monoclonal antibody," *Chemical Research in Toxicology*, vol. 4, no. 2, pp. 162–167, 1991.

[24] W. S. Sutherland and J. D. Winefordner, "Colloid filtration: a novel substrate preparation method for surface-enhanced Raman spectroscopy," *Journal of Colloid And Interface Science*, vol. 148, no. 1, pp. 129–141, 1992.

[25] A. O. Lundgren, F. Björefors, L. G. M. Olofsson, and H. Elwing, "Self-arrangement among charge-stabilized gold nanoparticles on a dithiothreitol reactivated octanedithiol monolayer," *Nano Letters*, vol. 8, no. 11, pp. 3989–3992, 2008.

[26] M. T. Rojas, R. Königer, J. F. Stoddart, and A. E. Kaifer, "Supported monolayers containing preformed binding sites: synthesis and interfacial binding properties of a thiolated β-cyclodextrin derivative," *Journal of the American Chemical Society*, vol. 117, no. 1, pp. 336–343, 1995.

[27] D. P. Griffis and R. W. Linton, "Effects of chemical state on quantitative AES of metal-sulfur compounds," *Surface and Interface Analysis*, vol. 6, no. 1, pp. 15–20, 1984.

[28] A. D. Becke, "Density-functional thermochemistry. III: the role of exact exchange," *The Journal of Chemical Physics*, vol. 98, no. 7, pp. 5648–5652, 1993.

[29] E. C. Le Ru and P. G. Etchegoin, *Principles of Surface-Enhanced Raman Spectroscopy and Related Plasmonic Effects*, Elsevier, Amsterdam, The Netherlands, 2009.

[30] N. M. B. Perney, J. J. Baumberg, M. E. Zoorob, M. D. B. Charlton, S. Mahnkopf, and C. M. Netti, "Tuning localized plasmons in nanostructured substrates for surface-enhanced Raman scattering," *Optics Express*, vol. 14, no. 2, pp. 847–857, 2006.

[31] E. J. Blackie, E. C. Le Ru, and P. G. Etchegoin, "Single-molecule surface-enhanced raman spectroscopy of nonresonant molecules," *Journal of the American Chemical Society*, vol. 131, no. 40, pp. 14466–14472, 2009.

[32] S. Shim, C. M. Stuart, and R. A. Mathies, "Resonance Raman cross-sections and vibronic analysis of rhodamine 6G from broadband stimulated raman spectroscopy," *ChemPhysChem*, vol. 9, no. 5, pp. 697–699, 2008.

[33] E. C. Le Ru, E. Blackie, M. Meyer, and P. G. Etchegoint, "Surface enhanced raman scattering enhancement factors: a comprehensive study," *Journal of Physical Chemistry C*, vol. 111, no. 37, pp. 13794–13803, 2007.

[34] R. J. J. Jansen and H. van Bekkum, "XPS of nitrogen-containing functional groups on activated carbon," *Carbon*, vol. 33, no. 8, pp. 1021–1027, 1995.

[35] J. M. Lindquist, J. P. Ziegler, and J. C. Hemminger, "Photoelectron spectroscopy studies of the hydrogenation of cyanogen on Pt(111): comparison with HCN and ethylenediamine," *Surface Science*, vol. 210, no. 1-2, pp. 27–45, 1989.

[36] A. Pashutski and M. Folman, "Low temperature XPS studies of NO and N_2O adsorption on Al(100)," *Surface Science*, vol. 216, no. 3, pp. 395–408, 1989.

[37] B. J. Lindberg and J. Hedman, "Molecular spectroscopy by means of ESCA. VI. Group shifts for N, P and As compounds," *Chemica Scripta*, vol. 7, pp. 155–166, 1975.

[38] W. Liu, Y. Zhang, and X. Gao, "Interfacial supramolecular self-assembled monolayers of C_{60} by thiolated β-cyclodextrin on gold surfaces via monoanionic C_{60} ," *Journal of the American Chemical Society*, vol. 129, no. 16, pp. 4973–4980, 2007.

[39] M. Dhayal and D. M. Ratner, "XPS and SPR analysis of glycoarray surface density," *Langmuir*, vol. 25, no. 4, pp. 2181–2187, 2009.

[40] D. Velic, M. Knapp, and G. Köhler, "Supramolecular inclusion complexes between a coumarin dye and β-cyclodextrin, and attachment kinetics of thiolated β-cyclodextrin to gold surface," *Journal of Molecular Structure*, vol. 598, no. 1, pp. 49–56, 2001.

[41] M. Weisser, G. Nelles, P. Wohlfart, G. Wenz, and S. Mittler-Neher, "Immobilization kinetics of cyclodextrins at gold surfaces," *Journal of Physical Chemistry*, vol. 100, no. 45, pp. 17893–17900, 1996.

[42] Y. Domi, Y. Yoshinaga, K. Shimazu, and M. D. Porter, "Characterization and optimization of mixed thiol-derivatized β-cyclodextrin/pentanethiol monolayers with high-density guest-accessible cavities," *Langmuir*, vol. 25, no. 14, pp. 8094–8100, 2009.

[43] O. Egyed, "Spectroscopic studies on β-cyclodextrin," *Vibrational Spectroscopy*, vol. 1, no. 2, pp. 225–227, 1990.

[44] G. Nelles, M. Weisser, R. Back, P. Wohlfart, G. Wenz, and S. Mittler-Neher, "Controlled orientation of cyclodextrin derivatives immobilized on gold surfaces," *Journal of the American Chemical Society*, vol. 118, no. 21, pp. 5039–5046, 1996.

[45] A. Z. M. Badruddoza, L. Junwen, K. Hidajat, and M. S. Uddin, "Selective recognition and separation of nucleosides using carboxymethyl-β-cyclodextrin functionalized hybrid magnetic nanoparticles," *Colloids and Surfaces B: Biointerfaces*, vol. 92, pp. 223–231, 2012.

[46] T. Uno, K. Machida, and K. Hanai, "Infra-red spectra of sulphamide and sulphamide-d4," *Spectrochimica Acta*, vol. 22, no. 12, pp. 2065–2073, 1966.

[47] I. S. Ahuja, C. L. Yadava, and R. Singh, "STructural information on manganese(II), cobalt(II), nickeL(II), zinC(II) and cadmium(II) sulphate complexes with hexamethylenetetramine (a potentially tetradentate ligand) from their magnetic moments, electronic and infrared spectra," *Journal of Molecular Structure*, vol. 81, no. 3-4, pp. 229–234, 1982.

[48] J. O. Jensen, "Vibrational frequencies and structural determinations of hexamethylenetetraamine," *Spectrochimica Acta. Part A: Molecular and Biomolecular Spectroscopy*, vol. 58, no. 7, pp. 1347–1364, 2002.

[49] S. E. J. Bell and M. R. Mccourt, "SERS enhancement by aggregated Au colloids: effect of particle size," *Physical Chemistry Chemical Physics*, vol. 11, no. 34, pp. 7455–7462, 2009.

[50] M. Osawa, "Surface-enhanced infrared absorption," in *Near-Field Optics and Surface Plasmon Polaritons*, S. Kawata, Ed., pp. 163–187, Springer, Berlin, Germany, 2001.

[51] G. W. Lucassen, W. P. de Boeij, and J. Greve, "Polarization-sensitive CARS of excited-state rhodamine 6G: induced anisotropy effects on depolarization ratios," *Applied Spectroscopy*, vol. 47, no. 12, pp. 1975–1988, 1993.